Directed Self-Assembly by Photostimulation of an Amorphous Semiconductor Surface

Yevgeniy V. Kondratenko and Edmund G. Seebauer
Dept. of Chemical and Biomolecular Engineering, University of Illinois, Urbana, IL 61801

DOI 10.1002/aic.12229
Published online April 12, 2010 in Wiley Online Library (wileyonlinelibrary.com).

A method for nanoscale directed self-assembly is demonstrated that employs an amorphous semiconductor containing subcritical nuclei for crystallization. This strategy combines attractive features of top-down and bottom-up approaches by exploiting the self-organization capabilities latent in amorphous materials, but in a way that can be controlled by optical or electron beam exposure tools. The method was demonstrated with amorphous TiO_2 deposited on silicon, heated to 270°C, and exposed to low-level ultraviolet light. © 2010 American Institute of Chemical Engineers *AIChE J,* 56: 3206–3211, 2010

Keywords: titanium oxide, directed self-assembly, chemical vapor deposition, photostimulated diffusion, nanofabrication

Introduction

Fabrication technologies for micro- and nanoscale devices require special toolsets for miniaturization and organization of materials. Toolsets now in use have developed from two different strategies. The ''top-down'' strategy commonly used in microelectronic devices carves out structures using deposition, lithography, and etching. Exquisite control is possible, but this approach becomes complicated and very expensive as the size scale decreases. The ''bottom-up'' strategy creates structures from smaller subunits through thermodynamically driven self-assembly, and has been employed with diverse objects such as nanotubes,[1] nanoparticles for synthesis of photonic bandgap crystals,[2,3] antibodies on gold surface for immunosensing,[4] and miniature electrical components (solder dots, wires, dies, and diodes) for electrical networks.[5,6] Cost is greatly reduced, but reliable control over patterning remains problematic due to entropy effects that become prominent at small length scales. The present work employs amorphous titanium dioxide to demonstrate principles underlying a hybrid approach that combines attractive features of both strategies. The approach exploits the self-organization capabilities latent in amorphous semiconductors, but in a way that is controllable by optical or electron beam exposure.

Correspondence concerning this article should be addressed to E. G. Seebauer at eseebaue@illinois.edu.

Concept of the method

The basic idea depends upon two attributes of solid semiconductors that have been discovered only within the past decade: photo-enhanced surface diffusion and ''medium range order.'' Low-level photostimulation has been shown to affect the diffusion of certain adsorbates on crystalline semiconductor surfaces such as Si(111) by nearly an order of magnitude.[7,8] Photostimulation changes the average charge state of surface point defects such as vacancies, which in turn propagates into the diffusion rate of adsorbates whose diffusion is mediated by those defects. Equivalent effects should occur with electron beam stimulation (although this phenomenon has not yet been demonstrated). The ''medium range order''[9] represents a special kind of atomic configuration within amorphous semiconductors. The atoms are arranged into topologically crystalline grains, roughly 1 nm in diameter, that are severely strained and therefore do not produce coherent diffraction or sharp Raman peaks. These grains can be thought of as subcritical nuclei for the growth of crystallites.

The self-assembly approach employs patterned exposure of an amorphous semiconductor to produce a spatially varying surface mass flux that, when performed at a temperature

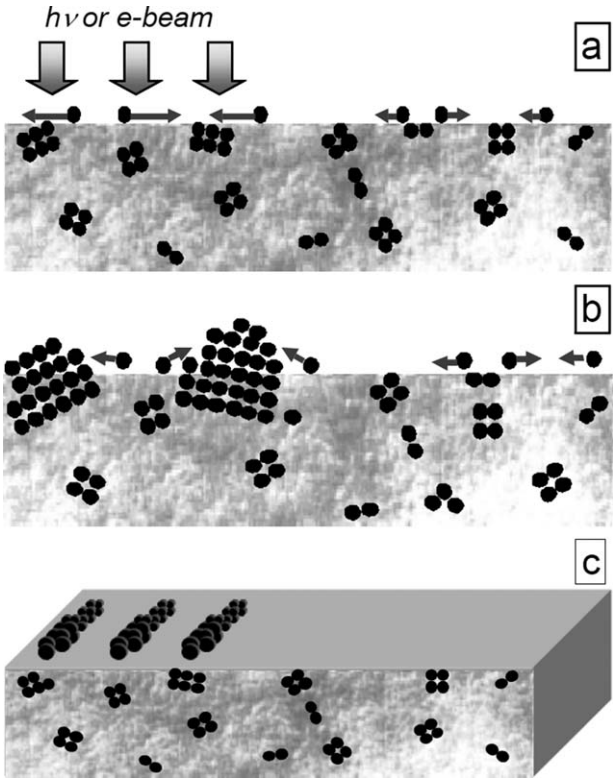

Figure 1. Schematic diagram of the directed self-assembly method.

(a) Surface of amorphous semiconductor containing subcritical nuclei is held just below the temperature of crystallization and exposed to a beam of photons or electrons. (b) In the exposed region, the increased rate of mass transport due to changes in average charge state of mobile atoms causes some subcritical nuclei to become supercritical and grow. Ostwald ripening prevents the formation of more nuclei. (c) Structures of 2–200+ nm can be formed depending on pattern and degree of Ostwald ripening permitted.

just below the cusp of crystallization, provides the extra nudge required to crystallize the subcritical nuclei in the exposed regions (Figure 1a). A related approach for stimulating and controlling localized order is already well known in the formation of hemispherical grained silicon for memory devices.[10,11] In that application, crystalline grains form on the amorphous Si (a-Si) surface when the material is annealed briefly at temperatures slightly above the cusp of crystallization. However, the crystallites thus formed are spatially random; the present approach seeks positional control.

With full-fledged crystallites created, the remaining amorphous film self-organizes by surface diffusion and Ostwald ripening (Figure 1b) until the desired structures are built up (Figure 1c). The size of the structures can be controlled by the heating time, the thickness of the original amorphous film, or both. Dot structures can be fabricated by point-like exposure. Walls can be fashioned by line exposure. Although initial nucleation of such walls occurs as a line of dots, subsequent grain growth causes the dots to merge. Important benefits of this approach become most evident when controlled types and numbers of irregularities must be introduced into an otherwise ordered structure. In a photonic band gap material, for example, a point defect acts like a cavity, a line defect like a waveguide, and a planar defect like a mirror.[12] Photonic band gap materials retain many of their desirable optical properties down to only four unit cells in thickness,[13] meaning that irregularities introduced into a nanoparticle template layer for colloidal particle deposition can propagate throughout the entire layer.

To implement the self-assembly approach requires an amorphous semiconductor that contains medium range order and for which surface diffusion can be enhanced at modest levels of stimulation. Medium range order has been detected in a wide variety of amorphous materials, including tetrahedral semiconductors (Ge and Si),[14–16] oxides (SiO_2 and GeO_2)[17] and even ternary[18] and quaternary glasses.[19] Indeed, the degree of such ordering can be controlled in a-Si with considerable precision through appropriate processing methods.[20,21] Surface diffusion on crystalline semiconductors that is enhanced by optical (or electron) stimulation was postulated[22] in the early 1990s and then observed[7,8] for photoexcitation a few years later. Analogous effects have yet not been reported for amorphous semiconductors. However, studies by photoemission spectroscopy have shown that atoms on a-Si surfaces can assume multiple charge states.[23] Such states are needed to influence diffusion nonthermally, so it is reasonable to believe that photoexcited diffusion can occur on amorphous semiconductors.

The present work employs amorphous TiO_2 (a-TiO_2) as the working material. Several properties of amorphous TiO_2 make it a particularly favorable candidate for success. There exists strong evidence for medium range order in titania-silica mixed glasses, based on neutron scattering experiments interpreted by Monte Carlo simulations.[24] The 3-eV band gap of TiO_2 means that the background carrier concentration is low. Hence, low levels of stimulation should be sufficient to significantly change the concentration of these carriers.

The literature for surface diffusion on amorphous materials is sparse,[25] especially for semiconductors, and no prior work exists for TiO_2. We therefore needed to characterize surface diffusion on a-TiO_2 in the dark before controlled photostimulation could be attempted. Fortunately, measurements of crystalline grain growth can themselves be employed to quantify surface diffusion. We employed methodology similar to that already developed for a-Si.[26,27] The results show that a-TiO_2 behaves similarly in many respects.

Above the crystallization temperature, grains nucleate spontaneously and grow in hemispherical shapes. For constant diffusional fluxes to the crystallite edges and self-similar hemispherical shapes during growth, the grain area depends linearly on time. Figure 2 demonstrates that a plot of average squared grain radius versus time is indeed linear, thereby indicating diffusion-limited growth. Grain growth took place at 200–300°C, however, compared to 550–650°C for a-Si. As with a-Si grown by CVD,[27] a-TiO_2 exhibited an induction time for initial nucleation of crystallization (450s at 270°C). However, analysis of the grain size distribution for TiO_2 showed that all grains nucleated simultaneously. Figure 3 shows that all potential grains had nucleated at the beginning of the annealing process (the smallest grains disappear after longer annealing), and the symmetric shape of the distribution further indicated the absence of continuous nucleation. Silicon, by contrast, exhibits continual nucleation resulting in a flatter size distribution.[28]

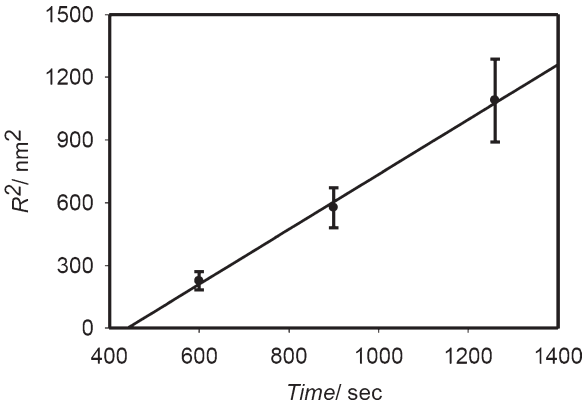

Figure 2. Average squared grain radius versus annealing time at 270°C.

Linear fit is evidence for growth kinetics limited by surface diffusion. Note the induction time of 440 seconds.

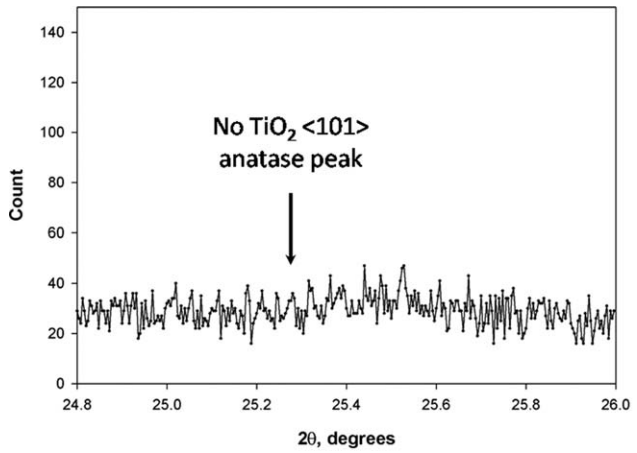

Figure 4. XRD spectrum of amorphous TiO_2 substrate grown at 190°C.

Experiment

Amorphous TiO_2 films of 120 nm thickness were grown in a stainless steel chamber on Si <100> substrates via low-pressure chemical vapor deposition. The substrates of approximate dimensions 1 cm × 1.5 cm were mounted between Ta clips for resistive heating during film growth and subsequent annealing. Partial pressures of the source gases were $2.0 \pm 0.1 \times 10^{-4}$ torr $TiCl_4$ and $6.0 \pm 0.1 \times 10^{-4}$ torr H_2O. Deposition lasted 1 hr at 150°C ± 1°C. X-ray diffraction confirmed that the as-grown films were amorphous (Figure 4). During annealing, the TiO_2 was exposed to low-level photostimulation of ~500 mW/cm^2 from a Xe arc lamp directed through glass filters selected to pass wavelengths of only 350–400 nm. Thermocouple measurements showed that the substrate temperature increased by less than 2°C during photostimulation. This point is important, as it rules out spurious diffusion effects caused by optically-induced heating. Indeed, a very similar configuration was used to detect optically induced inhibition of diffusion on crystalline silicon surfaces.[7]

For spatially-resolved photostimulation, specimens were shadowed in part by a Ta foil positioned within 1 mm of the surface. Exposure to the atmosphere passivates the surface to some extent. This fact was used to accentuate the effect of illumination on nucleation and growth (Figure 5), where the sample was exposed to atmosphere, thereby producing more vivid contrast between illuminated and dark sides. For elucidation of temperature effects on grain growth, the samples were annealed after purging the chamber with nitrogen without atmospheric exposure. This procedure significantly shortened experimental time while yielding acceptable numbers of grains.

Software distributed by Scion Corporation was used to obtain the grain concentration and size distribution from the SEM micrographs. From the grain areas, the grain radii were computed assuming a circular shape. Average R^2_{grain} was plotted versus time; the slope of the linear fit yielded the diffusional flux of atoms.

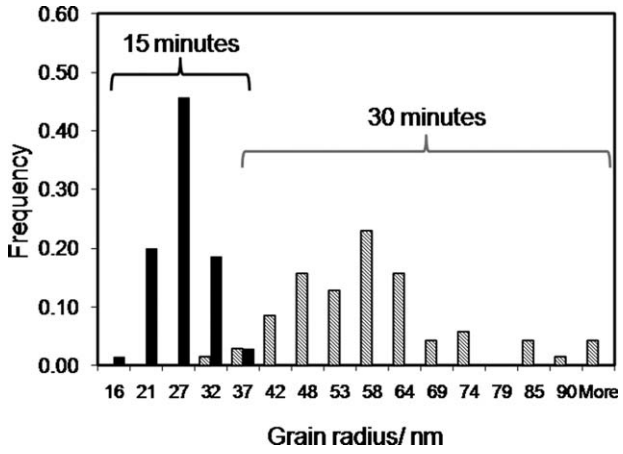

Figure 3. Grain radii distribution at different time intervals during annealing at 270°C.

Results

Surface diffusion

Diffusive transport for TiO_2 was quantified according to a model already developed for a-Si.[26] In brief, the lower surface energy of the crystallites draws mobile atoms from the surrounding amorphous surface. The model hypothesizes that an amorphous surface has a continuum of residuum defects, which generate mobile adatoms. These adatoms provide the greatest contribution to the surface diffusion.[25,27] These mobile atoms are replenished both by diffusion from further distances and by thermal generation of mobile atoms from defect-like structures in the amorphous surface. Since the grains are all hemispherical in shape, grain growth is almost certainly dominated by diffusion of mobile atoms over the amorphous surface rather than over the crystalline grain surface.

Fick's law describes the diffusion of the mobile atoms in a concentration gradient near the edge of a grain boundary, with the grain radius R growing slowly and to be treated simply as a parameter of the time t. The following mass balance relates the flux of diffusing species J to growth rate of the grain:

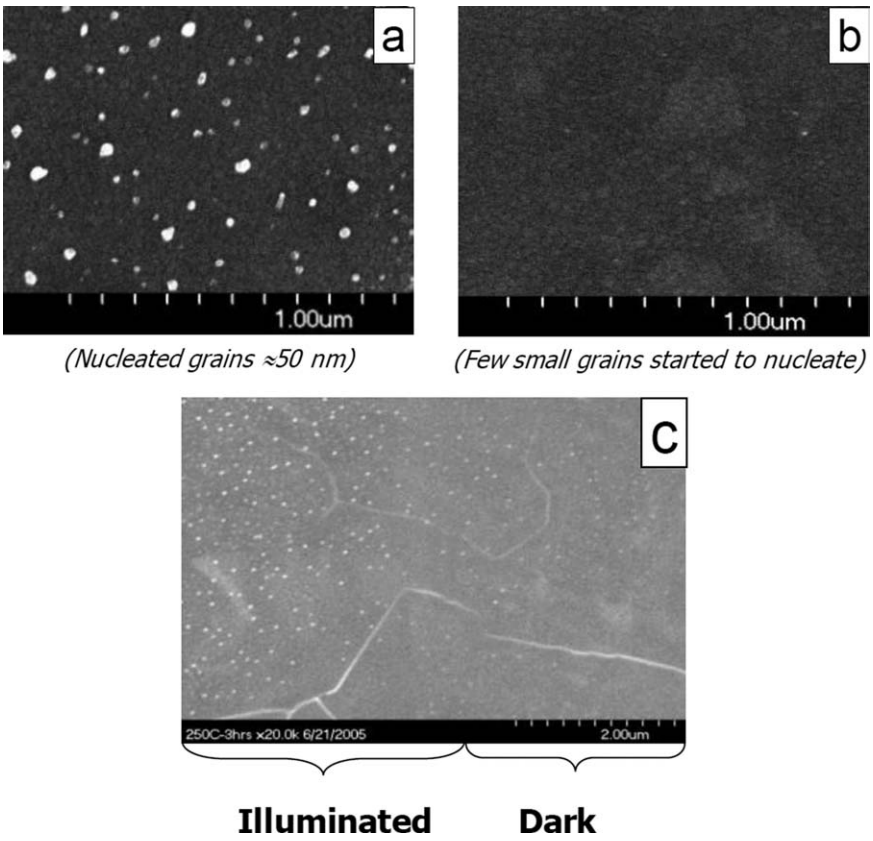

Figure 5. Nonthermally photostimulated enhancement of nucleation on amorphous TiO_2 during annealing for 3 hours at 250°C.

Grains nucleated and grow in the illuminated area (a), while the dark area (b) contains few grains. Grain density rapidly decays in the transition from illuminated to the dark area (c).

$$2\pi R^2 \frac{dR}{dt} = \frac{2\pi R}{C_b} J(R,t) \tag{1}$$

where C_b is the bulk crystal density (5.0×10^{22} cm^{-3}).

Considering that the characteristic decay time is several orders of magnitude shorter than experimental time, the flux can then be calculated from the pseudo-steady state solution:

$$J(R) = D_M C_{sub} \lambda \frac{K_1(\lambda R)}{K_0(\lambda R)} \tag{2}$$

with

$$\lambda = \sqrt{\frac{2\pi C_R}{\ln\left\{0.5(C_R/C_{sub})^{1/2}\right\}}} \tag{3}$$

where D_M denotes the mesoscale diffusivity of mobile atoms, which incorporates both the site-to-site hopping diffusivity of the mobile species and their concentration. C_{sub} denotes the areal concentration of substrate atoms on the amorphous surface, and C_R denotes the areal concentration of the defect-like structures that generate the mobile atoms. Eq. 2 indicates that the concentration of mobile atoms near a growing grain decays over a characteristic length λ. This length, together with D_M, can be extracted from fits of the experimental data for grain growth. The adatom hop length λ has been shown to be independent of temperature as well as the activation energy for Si, and that dependence is assumed here for TiO_2 as well.[8] As a result, λ can be treated essentially as a constant for the diffusivity measured in a narrow temperature window.[26]

Average grain radii were used for determining the flux based on a quasi-steady state model already developed.[26] The linear least squares method was used to minimize the difference between experimental and modeled flux, yielding the values of the fitting parameters D_M and λ.

For a-TiO_2 at 270°C, this analysis yields $D_M = 53$ cm^2/s $\pm$ 9 cm^2/s and $\lambda = (7 \pm 3) \times 10^6$ cm^{-1} The only directly comparable results in the literature are for λ, which for a-Si has the similar value $\lambda = 5 \times 10^6$ cm^{-1},[1,26] though in a higher temperature range of 525–590°C.

Directed self-assembly

Photostimulation effects can in principle affect grain nucleation, growth rate, or both. SEM imaging showed that photostimulation under the low intensity conditions of our experiment (0.5 W/cm^2) indeed affected nucleation and

growth rate. Figure 5a shows that grain density in the dark area was five grains/μm^2, while illumination increased nucleated grain density to 61 grains/μm^2. Furthermore, illuminated grains grew up to 10–50 nm in diameter, while grains in the dark area did not exhibit such growth. In fact, measurements of grain radii in the dark area were not possible due to limitation of SEM resolution for such small grains.

Shadowing part of the surface yielded spatially resolved nucleation as in Figure 5c. Numerous grains appear in the illuminated region, with very few in the dark region. In this case, nuclei were permitted to grow to a diameter of only 50 nm or so. However, continued annealing permitted them to grow much larger. The grains eventually flattened as their lateral diameter exceeded the amorphous layer thickness, and they merged when they were sufficiently close or the annealing time was sufficiently long. The pattern used in Figure 5c was extremely simple, and no attempt was made to create more sophisticated patterns with higher spatial resolution to create structures grain-by-grain. However, the basic idea behind the directed self-assembly approach outlined in Figure 1 has been demonstrated.

Discussion

The present method uses a small nonthermal stimulus to nudge selected regions into order that are already very close to organizing on their own. Not surprisingly, the results depend sensitively upon deposition and annealing temperatures. Crystalline grain concentration in the annealed material varies in accord with the concentration of subcritical nuclei in the original amorphous matrix. The latter concentration increases with increasing deposition temperature, as shown in the case of a-Si.[21] At sufficiently low temperatures, the material develops very few nuclei that can grow during annealing. But at high temperatures, the depositing film simply crystallizes spontaneously. For TiO_2, the practical upper and lower temperatures for deposition were $\sim$170°C and 100°C. These temperatures are good estimates for the upper and lower bounds on temperatures for subsequent annealing as well.

Other methods have been employed for directed self-assembly, including surface templating[2,3,29] and adaptations of photolithography.[30,31] However, the surface templating employs conventional lithographic or micromachining methods for patterning specific features onto the surface. After this patterning step, molecules or particles are then deposited with local ordering. Photolithography has also been used to remove unwanted portions of a uniformly deposited self-assembled layer. These approaches combine elements of top-down and bottom-up fabrication. But micromachining has limited spatial resolution, and adaptations of photolithography have the same weaknesses of expense and complication that lithography entails in conventional top-down fabrication.

The present approach avoids the need for resists and etching, and offers better spatial resolution than micromachining. Optical exposure suffers its own limits, but these can be circumvented if electron beam irradiation is used to stimulate diffusion. Low-level electron beams affect surface electron richness (as in cathodoluminescence[32]) and should affect the average charge state of mobile atoms and defects in a manner akin to photostimulation. Indeed, roughly analogous phenomena occur in bulk a-Si; electron beam irradiation of hydrogenated a-Si efficiently promotes the formation of metastable electronic defects.[9] The mechanism is thought to be the formation of charge carriers, rather than damage caused by electron collisions; electron beam exposure is thus equivalent to optical illumination.

Conclusion

The approach to directed self-assembly described here should be capable of producing single-layer particle arrays for sensors,[33] solar cells,[34] high-density/low-power storage media,[35] and other electronic devices.[36,37] The arrays can also be employed as ordered seed layers for the subsequent deposition of sintered particle films. Such films have been investigated for use in several applications, including the fabrication of flat panel displays[38] and related electrochromic devices, solar cells,[39] and rechargeable batteries.[38] Additional uses include advanced ceramics,[38] photonic band gap materials,[40] and gas sensors.[41] Currently, sintered particle films are manufactured by processes that rarely impart any special order upon the particles. However, when the films become sufficiently thin, order imposed by an initial seed layer can propagate throughout the film when subsequent layers are deposited by colloidal techniques.[42,43] Certain beneficial film properties, particularly optical properties,[12,34,42] become most pronounced with specific kinds of particle ordering. Templating using a suitably chosen pattern in the seed layer offers the possibility of tailoring this ordering.

Acknowledgments

This work was partially supported by NSF (CTS 02-03237 and DMR 07-04354) and the ACS PRF (43651-AC5). Electron microscopy was performed at the UIUC Center for Microanalysis of Materials, which is partially supported by the U.S. Department of Energy under grant DEFG02-96-ER45439.

Literature Cited

1. Blau WJ, Fleming AJ. Designer nanotubes by molecular self-assembly. *Science*. 2004;304:1457–1458.
2. Xia D, Biswas A, Li D, Brueck SRJ. Directed self-assembly of silica nanoparticles into nanometer-scale patterned surfaces using spin-coating. *Adv Mater*. 2004;16:1427–1432.
3. Phely-Bobin TS, Muisener RJ, Koberstein JT, Papadimitrakopoulos F. Preferential self-assembly of surface-modified Si/SiO_x nanoparticles on UV/ozone micropatterned poly(dimethylsiloxane) films. *Adv Mater*. 2000;12:1257–1261.
4. Vikholm I. Self-assembly of antibody fragments and polymers onto gold for immunosensing. *Sens Actuators B: Chem*. 2005;106:311–316.
5. Zheng W, Jacobs HO. Self-assembly process to integrate and connect semiconductor dies on surfaces with single-angular orientation and contact-pad registration. *Adv Mater*. 2006;18:1387–1392.
6. Gracias DH, Tien J, Breen TL, Hsu C, Whitesides GM. Forming electrical networks in three dimensions by self-assembly. *Science*. 2000;289:1170–1172.
7. Ditchfield R, Llera-Rodriguez D, Seebauer EG. Nonthermal effects of photon illumination on surface diffusion. *Phys Rev Lett*. 1998;81:1259–1262.
8. Ditchfield R, Llera-Rodriguez D, Seebauer EG. Semiconductor surface diffusion: nonthermal effects of photon illumination. *Phys Rev B*. 2000;61:13710–13720.
9. Diehl F, Herbst W, Bauer S, Schroder B, Oechsner H. Creation of metastable defects in a-Si:H by keV-electron irradiation at different temperatures. *J Non-Cryst Solids*. 1996;198–200(Part 1):436–440.

10. Watanabe H, Tatsumi T, Ikarashi T, Sakai A, Aoto N, Kikkawa T. An advanced technique for fabricating hemispherical-grained (HSG) silicon storage electrodes. *Electron Devices IEEE Trans*. 1995;42:295–300.
11. Suzuki K. Hemispherical-grained LPCVD-polysilicon films for use in MEMS applications. *Sensors Actuators A: Phys*. 2000;79:141–146.
12. Joannopoulos JD. The almost magical world of photonic crystals. *Proc IEEE Lasers Electro-Optics Soc*. 1999;1:232–233.
13. Leonard SW, Busch K, John S, van Driel HM, Birner A, Gosele U. Dependence of transmission on number of rows of 2-D macroporous silicon photonic band gap material. In: *IQEC, International Quantum Electronics Conference Proceedings*. 1999:267–268.
14. Treacy MMJ, Gibson JM, Keblinski PJ. Paracrystallites found in evaporated amorphous tetrahedral semiconductors. *J Non-Cryst Solids*. 1998;231:99–110.
15. Treacy MMJ, Voyles PM, Gibson JM. Schlafli cluster topological analysis of medium range order in paracrystalline amorphous semiconductor models. *J Non-Cryst Solids*. 2000;266–269(Part 1):150–155.
16. Bodapati A, Treacy MMJ, Falk M, Kieffer J, Keblinski P. Medium range order and the radial distribution function. *J Non-Cryst Solids*. 2006;352:116–122.
17. Gaskell PH. Medium-range structure in glasses and low-Q structure in neutron and X-ray scattering data. *J Non-Cryst Solids*. 2005;351:1003–1013.
18. Fan C, Wilson TW, Dmowski W, Choo H, Richardson JW, Maxey ER, Liaw PK. Quenched-in quasicrystal medium-range order and pair distribution function study on Zr55Cu35Al10 bulk metallic glass. *Intermetallics*. 2006;14:888–892.
19. Conradt R. Chemical structure, medium range order, and crystalline reference state of multicomponent oxide liquids and glasses. *J Non-Cryst Solids*. 2004;345–346:16–23.
20. Yu KM, Walukiewicz W, Muto S, Jin H-C, Abelson JR. The effects of x-ray induced structural changes on the microstructure of a-Si after thermal crystallization. *Appl Phys Lett*. 1999;75:2032–2034.
21. Voyles PM, Gerbi JE, Treacy MMJ, Gibson JM, Abelson JR. Increased medium-range order in amorphous silicon with increased substrate temperature. *J Non-Cryst Solids*. 2001;293–295:45–52.
22. Schultz KA, Seebauer EG. Surface diffusion of Sb on Ge(111) monitored quantitatively with optical second harmonic microscopy. *J Chem Phys*. 1992;97:6958–6967.
23. Winer K, Ley L. Near-surface electronic properties of a-Si:H. In: Fritzsche H, editor. *Amorphous Silicon and Related Materials*. Singapore: World Scientific Publication, 1989:365.
24. Pickup DM, Sowrey FE, Drake KO, Smith ME, Newport RJ. New insights into medium-range order around titanium in sol-gel derived silica through isotope difference neutron diffraction and reverse Monte Carlo modelling. *Chem Phys Lett*. 2004;392:503–507.
25. Seebauer EG, Allen CE. Estimating surface diffusion coefficients. *Prog Surf Sci*. 1995;49:265–330.
26. Dalton AS, Llera-Hurlburt D, Seebauer EG. Surface diffusion kinetics on amorphous silicon. *Surf Sci*. 2001;494:L761–L766.
27. Llera-Hurlburt D, Dalton AS, Seebauer EG. Temperature-dependent surface diffusion parameters on amorphous materials. *Surf Sci*. 2002;504:244–252.
28. Dalton AS. *Grain nucleation and growth on amorphous silicon*. University of Illinois, Urbana-Champaign, 2005.
29. Lu N, Gleiche M, Zheng J, Lenhert S, Xu B, Chi L, Fuchs H. Fabrication of chemically patterned surfaces based on template-directed self-assembly. *Adv Mater*. 2002;14:1812–1815.
30. Kan EC, Liu Z. Directed self-assembly process for nano-electronic devices and interconnect. *Superlattices Microstruct*. 2000;27:473–479.
31. Anderson ME, Srinivasan C, Hohman JN, Carter EM, Horn MW, Weiss PS. Combining conventional lithography with molecular self-assembly for chemical patterning. *Advanced Materials*. 2006;18:3258–3260.
32. Qian L, Teng F, Yang S, Quan S. Mixed excitation mechanism in solid-state cathodoluminescence structure. *Chem Phys Lett*. 2005; 405:389–392.
33. Musil CR, Jeggle D, Lehmann HW, Scandella L, Gobrecht J, Dobeli M. Nanostructuring of gold electrodes for immunosensing applications. *J Vacuum Sci Technol B*. 1995;13:2781–2786.
34. Yae S, Inakanishi I, Nakato Y, Toshima N, Mori H. Preparation of a langmuir-blodgett layer of ultrafine platinum particles and its application to N-Si for efficient photoelectrochemical solar-cells. *J Electrochem Soc*. 1994;141:3077–3081.
35. O'Barr R, Yamamoto SY, Schultz S, Weihua X, Scherer A. Fabrication and characterization of nanoscale arrays of nickel columns. *J Appl Phys*. 1997;81:4730–4732.
36. Datta S, Janes DB, Andres RP, Kubiak CP, Reifenberger RG. Molecular ribbons. *Semicond Sci Technol*. 1998;13:1347–1353.
37. Kan EC, Liu ZT. Directed self-assembly process for nano-electronic devices and interconnect. *Superlattices Microstruct*. 2000;27:473–479.
38. Fitz-Gerald J, Singh RK. Novel method for synthesis of engineering particulates with thin coatings. *Surf Controlled Nanoscale Mater High Value Add Appl*. 1998;501:363–368.
39. Gratzel M. Photovoltaics: state of the art and perspectives for nanocrystalline injection cells. *EI Elektrotechnik und Informationstechnik*. 1997;114:579–586.
40. Scalora M, Bloemer MJ, Bowden CM. Metals under a new light. *Optics Phototonics News*. 1999;10:24–27.
41. Vacassy R, Houriet R, Plummer CJC, Dutta J, Hoffmann H. Tin dioxide nanopowders for gas sensor applications. *Surf Controlled Nanoscale Mater High Value Add Appl*. 1998;501:41–46.
42. Pileni MP. Fabrication and properties of nanosized material made by using colloidal assemblies as templates. *Cryst Res Technol*. 1998;33:1155–1186.
43. Lin KH, Crocker JC, Prasad V, Schofield A, Weitz DA, Lubensky TC, Yodh AG. Entropically driven colloidal crystallization on patterned surfaces. *Phys Rev Lett*. 2000;85:1770–1773.

Manuscript received Aug. 14, 2009, revision received Oct. 31, 2009, and final revision received Feb. 22, 2010.